Thermoelectric properties of semiconductor-metal composites produced by particle blending

Yu Liu, Doris Cadavid' , Maria Ibáñez, Silvia Ortega, Sara Martí-Sánchez, Oleksandr Dobrozhan, Maksym V. Kovalenko, Jordi Arbiol, and Andreu Cabot'

Citation: APL Materials **4**, 104813 (2016); doi: 10.1063/1.4961679
View online: http://dx.doi.org/10.1063/1.4961679
View Table of Contents: http://aip.scitation.org/toc/apm/4/10
Published by the American Institute of Physics

Thermoelectric properties of semiconductor-metal composites produced by particle blending

Yu Liu,[1] Doris Cadavid,[1,a] Maria Ibáñez,[2,3] Silvia Ortega,[1] Sara Martí-Sánchez,[4] Oleksandr Dobrozhan,[1] Maksym V. Kovalenko,[2,3] Jordi Arbiol,[4,5] and Andreu Cabot[1,5,a]

[1]*Catalonia Institute for Energy Reseach-IREC, Sant Adrià de Besòs, 08930 Barcelona, Spain*
[2]*Department of Chemistry and Applied Biosciences, Institute of Inorganic Chemistry, ETH Zürich CH-8093, Switzerland*
[3]*Empa-Swiss Federal Laboratories for Materials Science and Technology, Dübendorf CH-8600, Switzerland*
[4]*CSIC and The Barcelona Institute of Science and Technology, Catalan Institute of Nanoscience and Nanotechnology (ICN2), Bellaterra, 08193 Barcelona, Catalonia, Spain*
[5]*ICREA, Pg. Lluís Companys 23, 08010 Barcelona, Spain*

(Received 30 April 2016; accepted 15 August 2016; published online 29 August 2016)

In the quest for more efficient thermoelectric material able to convert thermal to electrical energy and vice versa, composites that combine a semiconductor host having a large Seebeck coefficient with metal nanodomains that provide phonon scattering and free charge carriers are particularly appealing. Here, we present our experimental results on the thermal and electrical transport properties of PbS-metal composites produced by a versatile particle blending procedure, and where the metal work function allows injecting electrons to the intrinsic PbS host. We compare the thermoelectric performance of composites with microcrystalline or nanocrystalline structures. The electrical conductivity of the microcrystalline host can be increased several orders of magnitude with the metal inclusion, while relatively high Seebeck coefficient can be simultaneously conserved. On the other hand, in nanostructured materials, the host crystallites are not able to sustain a band bending at its interface with the metal, becoming flooded with electrons. This translates into even higher electrical conductivities than the microcrystalline material, but at the expense of lower Seebeck coefficient values. [http://dx.doi.org/10.1063/1.4961679]

The cost-effective use of solid state thermoelectric devices to directly convert heat to electricity and vice versa requires designing and engineering thermoelectric materials that provide higher performance. In this direction, composites offer several advantages.[1–8] The thermal conductivity of composite materials can be strongly reduced with respect to their components by effective phonon scattering at the interfaces of two dissimilar materials. Additionally, high charge carrier concentrations can be reached while conserving high carrier mobilities by modulation doping, that is, by introducing electronic dopants in just one of the phases and spilling the carriers over from this phase to the host semiconductor. This doping strategy minimizes the influence of ionized doping impurities on charge carrier transport when this takes place through the other phase.[9] Furthermore, higher Seebeck coefficients can be obtained by selectively scattering low energy charge carriers at interfaces.[10] Alternatively, by properly selecting the constituent materials and precisely engineering the composite, the minority phase can become invisible to charge carriers.[11–13] Besides, in particular cases, inclusions can even improve charge carrier mobility by reducing intergrain potential barriers in the matrix material, as recently observed in semiconductor-metal nanocomposites.[14]

[a]Authors to whom correspondence should be addressed. Electronic addresses: dcadavid@irec.cat and acabot@irec.cat

This last type of composite, obtained from combining a semiconductor host having a large Seebeck coefficient with metal inclusions, is particularly interesting. A potentially strong acoustic impedance mismatch between the semiconductor and the metal provides a very efficient interface phonon scattering. Besides, the very high density of free carriers in metals represents a convenient charge pool to adjust the host charge carrier concentration if a proper band alignment for charge spillover exists.[14,15] Additionally, Schottky metal-semiconductor interfaces may effectively and preferentially scatter low energy carriers.[10,16] The interest that semiconductor-metal composites has evoked is such that in the last decade a wide spectrum of experimental results, not always obviously consistent between each other, has been reported for several different combinations (Table I).

The proper design and engineering of a semiconductor-metal composite requires not only to select materials with a suitable band alignment but also to use production approaches that allow tuning the material composition and properly distributing the different phases. In this regard, the blending of metal and semiconductor particles in a controlled atmosphere represents an extremely simple methodology to produce composites with a huge compositional versatility and an excellent control over a number of parameters, such as distribution and composition of the phases. Within this approach, the particle sizes of both metal and semiconductor are the key parameters as they determine the final metal and semiconductor domain size in the composite and the metal domain density at a set overall composition. These parameters not only determine the extent of phonon scattering, charge spillover, or potential energy filtering but also the extent that the metal influences the host semiconductor Fermi level, especially when employing intrinsic semiconductors as those required to take full advantage of the modulation doping strategy.

TABLE I. Effect of the metal on semiconductor-metal composites as reported in the literature. Red: worsens; green: improves; yellow: unchanged; blue: no data.[14,15,17–35] κ is thermal conductivity, S the Seebeck coefficient, σ the electrical conductivity and, n and p are the carrier density according to the type of the semiconductor N or P.

Semiconductor	Metal	κ	S	σ	n/p	μ	Reference
PbS (N)	Ag						14
PbTe (P)	Pb						17
Bi_2Te_3 (N)	Au						18
Bi_2Te_3 (N)	Cu						19
Bi_2Te_3 (N)	Ag						20
Bi_2Te_3 (N)	Bi						21
Sb_2Te_3 (P)	Ag						22
Sb_2Te_3 (P)	Pt						22
$Bi_{0.5}Sb_{1.5}Te_3$ (N)	Cu						23
$Bi_{0.5}Sb_{1.5}Te_3$ (P)	Ag						24
$Bi_{0.5}Sb_{1.5}Te_3$ (P)	Cu						24
$Bi_2Te_{2.7}Se_{0.3}$ (N)	Pt						25
$Bi_2(Te_{0.9}Se_{0.1})_3$ (P)	Cu						26
$Bi_2(Te_{0.9}Se_{0.1})_3$ (P)	Zn						26
GaAs (N)	Bi						27
GaAs (N)	In						28
$FeSb_2$ (N)	Cu						15
$FeSb_2$ (N)	AgSb						29
$Ba_{0.3}Co_4Sb_{12}$ (N)	Ag						30
Na_xCoO_2 (P)	Au						31
$Bi_2Sr_2Co_2O_y$ (P)	Ag						32
$Ca_3Co_4O_{9+\delta}$ (P)	Ag						33
$Ca_3Co_4O_9$ (P)	Ag						34
$Na_xCo_2O_4$ (P)	Ag						35

We recently demonstrated that low work function metals such as Ag are able to inject electrons to a quasi-intrinsic and nanostructured PbS host.[14] We also observed that the presence of Ag at the interfaces allowed reducing the energy barriers for charge transport between PbS grains, thus not only minimizing the influence over mobility, as in a conventional modulation-doping scenario, but actually also improving it. In the present work, we demonstrate that combinations of intrinsic PbS with low work function non-noble metals, such as copper and tin, can also provide higher thermoelectric performances. Besides, here we compare the results obtained from a nanocrystalline semiconductor host, which Fermi level may be pinned to the metal's, with those of a microcrystalline host, which supports the band bending at the metal-semiconductor interface. We demonstrate that while higher electrical conductivities can be reached with a more extensive distribution of metal nanoparticles within the host semiconductor, larger Seebeck coefficients can be maintained with the microcrystalline host.

Cubic PbS nanocrystals with a mean edge size of ∼10 nm were prepared following our previously reported procedure.[36] Cu nanocrystals with an average diameter of ∼5 nm were prepared following the approach developed by Yang *et al.*[37] Sn nanocrystals with an average diameter of ∼13 nm were prepared using the method developed by Kovalenko *et al.*[38]

The blending of nanocrystals was performed by wetting 750 mg of dried PbS nanocrystals with different amounts of a solution of metal nanocrystals in anhydrous chloroform. Subsequently, the solvent was allowed to evaporate under the argon atmosphere.

Proper amounts of commercial PbS and Cu powders were mixed inside an argon-filled glovebox by manually grinding them with an agate mortar.

PbS-metal blends were annealed at 450 °C for 60 min under an Ar flow inside a tube furnace. Then, the annealed powder was loaded into a graphite die and compacted into pellets (Ø10 mm × 1.5 mm) in an Ar atmosphere using a custom-made hot press for 5 min at 420 °C and under 70 MPa pressure. The relative density of the obtained pellets was higher than 85% of the theoretical value in all cases.

X-ray diffraction (XRD) patters were obtained on a Bruker AXS D8 ADVANCE X-ray diffractometer with Cu–Kα radiation (λ = 0.154 06 Å). Transmission electron microscopy (TEM) characterization was carried out on a Zeiss Libra 120, operating at 120 kV. High resolution TEM (HRTEM) images were obtained using a Jeol 2010F field-emission gun microscope at 200 keV. Field-emission scanning electron microscopy (SEM) micrographs were obtained on Zeiss Auriga at 5.0 kV. Composition was analyzed by means of an Oxford energy dispersive X-ray (EDX) spectrometer coupled to the SEM.

Both the Seebeck coefficient and the electrical resistivity were measured simultaneously in a LSR-3 LINSEIS system under helium atmosphere. Thermal conductivities were calculated by $\kappa = \lambda C_p \rho$, where λ is the thermal diffusivity, C_p is the heat capacity, and ρ is the mass density of the specimen. Thermal diffusivities were measured using XFA 600 Xenon Flash apparatus. The specific heat (C_P) was calculated by the Dulong-Petit approximation, and the density values used were obtained using the Archimedes' method. Error bars were estimated from the repeatability of the experimental result obtained, calculated after measuring each parameter 3 times. Hall carrier concentrations were measured using a PPMS-9T from Quantum Design, Inc. at room temperature under a magnetic field of 2 T.

Figures 1(a)-1(d) display representative TEM micrographs and the corresponding particle size histograms of the 10 nm cubic PbS, the 5 nm spherical Cu, and the 13 nm spherical Sn nanocrystals obtained following the above procedures and used to produce semiconductor-metal nanocomposites. Figure 1(e) shows the nanocrystals XRD patterns. Importantly, no secondary phases, including the corresponding oxides, were detected when carefully producing, manipulating, and purifying the nanocrystals in air-free conditions.

PbS-Cu and PbS-Sn nanocomposites with adjusted metal concentrations were produced by combining purified PbS nanocrystals with different amounts of a suspension of colloidal Cu or Sn nanocrystals, respectively. To remove residual organic compounds and chemically and structurally stabilize the material, nanocomposites were annealed at 450 °C for 60 min under an Ar flow. Subsequently, the annealed powder was consolidated into disk-shaped pellets using a hot-press. EDX analysis showed the amount of Cu and Sn in the final nanocomposite to be consistent, within the

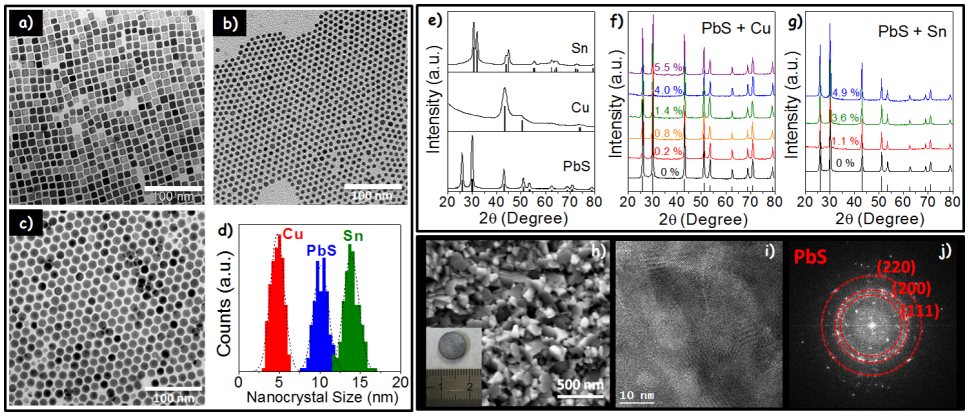

FIG. 1. (a)-(d) TEM micrographs of PbS (a), Cu (b), and Sn (c) nanocrystals and the corresponding size histograms (d). (e) XRD patterns of PbS, Cu, and Sn nanocrystals. The respective reference patterns are also plotted as follows: PbS: JCPDS 00-005-0592; Cu: JCPDS 03-065-9026; Sn: JCPDS 01-086-2265. (f)-(g) XRD patterns for different concentrations of Cu in the PbS-Cu (f) and PbS-Sn (g) nanocomposite pellets. (h) Representative SEM micrograph of a PbS-Sn nanocomposite showing 100-200 nm grains. Inset shows an image of the actual pellet. (i) HRTEM micrograph and (j) power spectra of the PbS-Sn nanocomposite showing the material polycrystallinity with crystal domain sizes in the range between 10 and 20 nm.

experimental error, with the nominal composition of the nanocomposites prepared. This result was to be expected as no additional purification process was performed after the nanocrystal combination, and processing temperatures were not high enough for metal evaporation.

Figures 1(f) and 1(g) show the XRD patterns of PbS-Cu and PbS-Sn nanocomposite pellets, respectively. Because of the low amount of metal introduced and the coincidence of the main x-ray diffraction peaks of the metal with those of PbS, the presence of metallic Cu and Sn phases was not detected by XRD. During the annealing processes, PbS grains were observed to grow from the initial 10 nm to around 100-200 nm (Figure 1(h)). However, careful HRTEM analysis showed the grains to be highly polycrystalline, with crystal domain sizes in the range 10–20 nm (Figures 1(i) and 1(j)). The coincidence of interplanar spacings did not allow obtaining evidences of the presence of metallic Cu or Sn crystals from HRTEM and electron diffraction.

The electrical conductivities (σ), Seebeck coefficients (S), thermal conductivities (κ), and dimensionless thermoelectric figure of merit $ZT = \sigma S^2 T/\kappa$ of nanocrystalline PbS and a series of PbS-Cu and PbS-Sn nanocomposites with metal concentrations up to 5 mol% are displayed in Figure 2. The pristine PbS material was characterized by low electrical conductivity at ambient temperature, which, as it corresponds to an intrinsic or poorly doped semiconductor, strongly

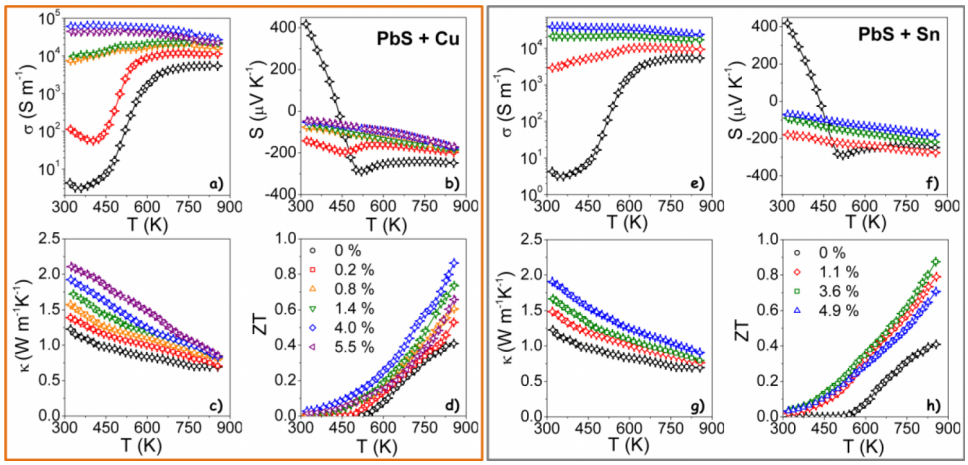

FIG. 2. Temperature dependence of the (a), (e) electrical conductivity, σ; (b), (f) Seebeck coefcient, S; (c), (g) thermal conductivity, κ; and (d), (h) thermoelectric figure of merit (ZT) for PbS-Cu (a)-(d) and PbS-Sn (e)-(h) nanocomposites.

increased with temperature. Consistently, relatively high Seebeck coefficients were measured for PbS at ambient temperature. Besides, a sign inversion in the Seebeck coefficient was observed at around 450 K, corresponding to a change from p-type to n-type conductivity. PbS–Cu and PbS-Sn nanocomposites showed significantly higher electrical conductivities, which increased with the metal content. For the nanocomposites with the highest metal contents, electrical conductivities decreased with temperature, as it corresponds to a degenerated semiconductor. This result demonstrates the important electronic role that Cu and Sn play on the final material. Over the entire temperature range measured, both PbS–Cu and PbS-Sn nanocomposites exhibited negative Seebeck coefficients and their absolute values increased with temperature. This n-type behavior pointed towards an injection of electrons from the metal to the host semiconductor. Consistently with the higher electrical conductivities measured, lower Seebeck coefficients were generally obtained for the nanocomposites when compared with pristine PbS.

Hall charge carrier concentration measurements provided further evidence of the charge carrier increase, of up to 3 orders of magnitude, obtained with the introduction of metal nanocrystals. The Hall charge carrier concentrations at room temperature for PbS, PbS-Cu 4 mol%, and PbS-Sn 3.6 mol% were $p = 2 \times 10^{16}$ cm^{-3}, $n = 3 \times 10^{19}$ cm^{-3}, and $n = 1 \times 10^{19}$ cm^{-3}, respectively. The majority carrier mobilities directly calculated from the measured electrical conductivities were $\mu_p = 14$ cm$^2 \cdot$ V$^{-1} \cdot$ s^{-1}, $\mu_n = 130$ cm$^2 \cdot$ V$^{-1} \cdot$ s^{-1}, and $\mu_n = 130$ cm$^2 \cdot$ V$^{-1} \cdot$ s^{-1}, for PbS, PbS-Cu 4 mol%, and PbS-Sn 3.6 mol%, respectively.

With the metal addition, higher thermal conductivities, which increased with the metal content, were obtained in the whole temperature range. This increase is associated with the higher electronic component of the thermal conductivity. Overall, nanocomposites displayed significantly higher power factors ($PF = \sigma S^2$) and figures of merit than pristine PbS. Maximum ZT values were obtained for PbS-Cu 4.0 mol% and PbS-Sn 3.6 mol% nanocomposites, which reached ZT values up to 0.86 and 0.88 at 855 K, respectively, which represents a twofold increase over pristine PbS. Higher metal concentrations provided either a too large reduction in the Seebeck coefficient or a too large increase on thermal conductivity, thus decreasing the overall thermoelectric figure of merit. To estimate measurement accuracy and have a first assessment of the sample stability, all measurements were repeated at least three times for each sample, providing minimal variations.

Figure 3 displays the results obtained from the thermoelectric characterization of microcrystalline PbS and PbS-Cu 4.0 mol% composites produced from commercial powders. Results are compared with those obtained from nanocrystalline PbS and the PbS-Cu 4.0 mol% nanocomposite produced from colloidal nanoparticles. Electrical conductivities of the pristine microcrystalline PbS were low, similar to those of the PbS nanomaterial. In the high temperature range, higher electrical conductivities were obtained for the nanocrystalline PbS, which we associate to a higher density of

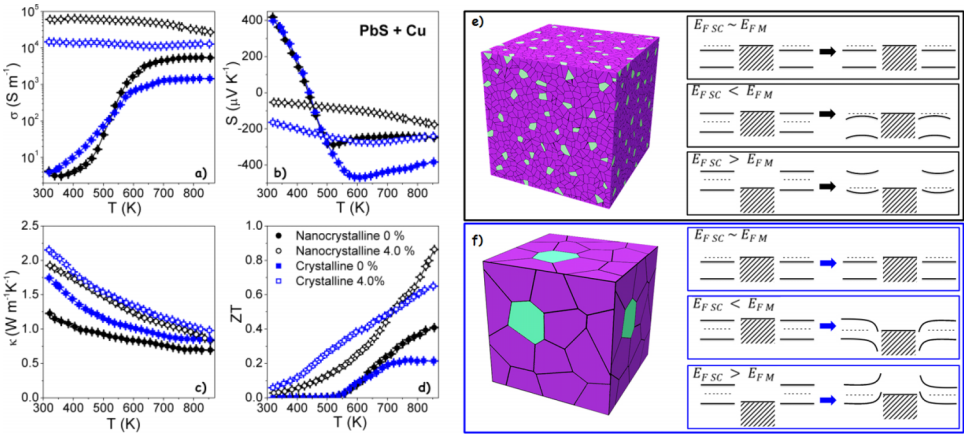

FIG. 3. Temperature dependence of the (a) electrical conductivity; (b) Seebeck coefficient; (c) thermal conductivity; and (d) thermoelectric figure of merit for microcrystalline PbS–Cu composites (blue squares) and PbS-Cu nanocomposites (black circles). (e)-(f) Scheme of a semiconductor-metal nanocomposite and a microcomposite and the band alignments in three scenarios depending on the relative position of the semiconductor ($E_{F\,SC}$) and metal Fermi Energy levels ($E_{F\,M}$).

surface defects, susceptible to be ionized in the high temperature range and thus providing higher charge carrier concentrations. With the Cu introduction, the electrical conductivities of the microcrystalline composite increased several orders of magnitude, up to 10^4 S m^{-1}, but remained a factor 4 lower than those of the PbS-Cu nanocomposite.

On the other hand, the Seebeck coefficients of the pristine PbS microcrystalline material showed a similar temperature evolution as the nanocrystalline PbS, but reached higher values in the high temperature range, which is consistent with the relatively lower electrical conductivities measured in this temperature range for the microcrystalline material. In the presence of copper, negative Seebeck coefficients were measured in the whole temperature range, which, together with the large increase of electrical conductivity, points toward a spillover of electrons from the metal to the host semiconductor, as in the case of the PbS-Cu nanocomposite. In the microcrystalline composite however, much higher Seebeck coefficients than in the nanocomposite were obtained, even when comparing with nanocomposites having lower Cu loads and similar electrical conductivities. We associate the relatively lower Seebeck coefficients obtained in the nanocrystalline material to the nanocrystals charge flooding, not being able to sustain a sufficient band bending due to their small size and low electronic doping. In the microcrystalline compound, the injection of charge from copper to PbS introduces a band bending in the semiconductor, but still most of the PbS crystal remains quasi-intrinsic, thus overall providing much larger Seebeck coefficients (Figures 3(e) and 3(f)).

In microcrystalline PbS, the measured Hall charge carrier concentration at room temperature was $p = 9 \times 10^{15}$ cm^{-3}, just slightly lower than for nanocrystalline PbS. The related charge carrier mobility was $\mu_p = 28$ $cm^2 \cdot V^{-1} \cdot s^{-1}$, twofold higher than in nanocrystalline PbS. When introducing a 4 mol% of Cu, the microcrystalline PbS-Cu 4 mol% composite displayed a charge carrier concentration of $n = 2 \times 10^{18}$ cm^{-3}, which was one order of magnitude lower than when blending the same amount of Cu with nanocrystalline PbS. From this carrier concentration value, the calculated mobility in the microcrystalline composite was 3-fold larger than that of the nanocomposite, which is consistent with the higher crystallinity of the former.

As expected, the thermal conductivities of the microcrystalline PbS and the PbS-Cu composite were larger than those of the nanocrystalline PbS and PbS-Cu. Overall, while larger ZT values were obtained for the microcrystalline compound in the low temperature range measured, due to the much higher Seebeck coefficients provided, in the high temperature range, the nanocomposite was characterized by higher ZT values related to the lower lattice thermal conductivity due to more efficient phonon scattering and the higher electrical conductivities associated to a more efficient charge carrier injection from the metal to the semiconductor.

PbS-Cu and PbS-Sn composites were prepared by a facile and extremely versatile approach consisting on blending the proper amount of particles of each components and subsequently hot-pressing the resulting mixture. Compared with pristine PbS, PbS-metal composites exhibited much higher electrical conductivities and negative Seebeck coefficients in the whole temperature range, consistent with a spillover of electrons from the low work function metal to the semiconductor. Due to the strong contribution of the electronic thermal conductivity, the metal addition had associated an increase of the thermal conductivity. When comparing the thermoelectric properties of PbS-Cu composites with crystal domain sizes in the micrometer scale with those of nanocomposites with dimensions of both components in the nanometer size regime, we observed that with the same metal loading, higher electrical conductivities were reached in the nanocomposite, but higher Seebeck coefficients were maintained in the microcomposite. Both results were associated to a more efficient charge transfer from the metal to the semiconductor in the nanocrystalline materials. As expected, lower thermal conductivities were also measured in the nanocomposite. Overall, higher ZT values were measured on the microcomposite in the low temperature range, but higher ZT values were measured from the nanocomposites in the higher temperature range. Both in microcomposites and nanocomposites, a 2-fold increase of ZT was obtained over pristine PbS.

This work was supported by the European Regional Development Funds, the Framework 7 program under project UNION (No. FP7-NMP-2012-310250), and the Spanish MINECO Project BOOSTER (No. ENE2013-46624-C4-3-R). Y.L. thanks the China Scholarship Council (No. CSC 201406500003) for the scholarship support. M.I., O.D., and S.O. thank AGAUR for their Beatriu

de Pinós postdoctoral Grant No. (2013 BP-A00344) and Ph.D. grants. M.V.K. acknowledges the partial financial support from the European Union (EU) via FP7 ERC Starting Grant 2012 (Project NANOSOLID, GA No. 306733). Authors also acknowledge the funding from Generalitat de Catalunya 2014 SGR 1638.

[1] A. M. Dehkordi, M. Zebarjadi, J. He, and T. M. Tritt, Mater. Sci. Eng., R **97**, 1–22 (2015).
[2] C. J. Vineis, A. Shakouri, A. Majumdar, and M. G. Kanatzidis, Adv. Mater. **22**, 3970–3980 (2010).
[3] M. Ibáñez, R. Zamani, S. Gorsse, J. Fan, S. Ortega, D. Cadavid, J. R. Morante, J. Arbiol, and A. Cabot, ACS Nano **7**, 2573–2586 (2013).
[4] J. R. Sootsman, D. Y. Chung, and M. G. Kanatzidis, Angew. Chem., Int. Ed. **48**, 8616–8639 (2009).
[5] Y. Zhang and G. D. Stucky, Chem. Mater. **26**, 837–848 (2013).
[6] Y. Lan, A. J. Minnich, G. Chen, and Z. Ren, Adv. Funct. Mater. **20**, 357–376 (2009).
[7] J. He, M. G. Kanatzidis, and V. P. Dravid, Mater. Today **16**, 166–176 (2013).
[8] L.-D. Zhao, V. P. Dravid, and M. G. Kanatzidis, Energy Environ. Sci. **7**, 251–268 (2014).
[9] M. Zebarjadi, G. Joshi, G. Zhu, B. Yu, A. Minnich, Y. Lan, X. Wang, M. Dresselhaus, Z. Ren, and G. Chen, Nano Lett. **11**, 2225–2230 (2011).
[10] S. V. Faleev and F. Léonard, Phys. Rev. B **77**, 214304 (2008).
[11] M. Zebarjadi, B. Liao, K. Esfarjani, M. Dresselhaus, and G. Chen, Adv. Mater. **25**, 1577–1582 (2013).
[12] W. Shen, T. Tian, B. Liao, and M. Zebarjadi, Phys. Rev. B **90**, 075301 (2014).
[13] J. Y. Lee and R.-K. Lee, Phys. Rev. B **89**, 155425 (2014).
[14] M. Ibáñez, Z. Luo, A. Genc, L. Piveteau, S. Ortega, D. Cadavid, O. Dobrozhan, Y. Liu, M. Nachtegaal, M. Zebarjadi, J. Arbiol, M. V. Kovalenko, and A. Cabot, Nat. Commun. **7**, 10766 (2016).
[15] M. Koirala, H. Zhao, M. Pokharel, S. Chen, T. Dahal, C. Opeil, G. Chen, and Z. Ren, Appl. Phys. Lett. **102**, 213111 (2013).
[16] J. M. O. Zide, J.-H. Bahk, R. Singh, M. Zebarjadi, G. Zeng, H. Lu, J. P. Feser, D. Xu, S. L. Singer, Z. X. Bian, A. Majumdar, J. E. Bowers, A. Shakouri, and A. C. Gossard, J. Appl. Phys. **108**, 123702 (2010).
[17] J. P. Heremans, C. M. Thrush, and D. T. Morelli, J. Appl. Phys. **98**, 063703 (2005).
[18] E. Lee, J. Ko, J.-Y. Kim, W.-S. Seo, S.-M. Choi, K. H. Lee, W. Shim, and W. Lee, J. Mater. Chem. C **4**, 1313–1319 (2016).
[19] F. R. Sie, C. H. Kuo, C. S. Hwang, Y. W. Chou, C. H. Yeh, Y. L. Lin, and J. Y. Huang, J. Electron. Mater. **45**, 1927–1934 (2016).
[20] Q. Zhang, X. Ai, L. Wang, Y. Chang, W. Luo, W. Jiang, and L. Chen, Adv. Funct. Mater. **25**, 966–976 (2015).
[21] S. Sumithra, N. J. Takas, D. K. Misra, W. M. Nolting, P. F. P. Poudeu, and K. L. Stokes, Adv. Energy Mater. **1**, 1141–1147 (2011).
[22] Y. Zhang, M. L. Snedaker, C. S. Birkel, S. Mubeen, X. Ji, Y. Shi, D. Liu, X. Liu, M. Moskovits, and G. D. Stucky, Nano Lett. **12**, 1075–1080 (2012).
[23] I.-H. Kim, S.-M. Choi, W.-S. Seo, and D.-I. Cheong, Nanoscale Res. Lett. **7**, 1–6 (2012).
[24] K.-H. Lee, H.-S. Kim, S.-I. Kim, E.-S. Lee, S.-M. Lee, J.-S. Rhyee, J.-Y. Jung, I.-H. Kim, Y. Wang, and K. Koumoto, J. Electron. Mater. **41**, 1165–1169 (2012).
[25] T. Sun, M. K. Samani, N. Khosravian, K. M. Ang, Q. Yan, B. K. Tay, and H. H. Hng, Nano Energy **8**, 223–230 (2014).
[26] S. Wang, H. Li, R. Lu, G. Zheng, and X. Tang, Nanotechnology **24**, 285702 (2013).
[27] M. V. Warren, J. C. Canniff, H. Chi, F. Naab, V. A. Stoica, R. Clarke, C. Uher, and R. S. Goldman, J. Appl. Phys. **117**, 065101 (2015).
[28] M. V. Warren, J. C. Canniff, H. Chi, E. Morag, F. Naab, V. A. Stoica, R. Clarke, C. Uher, and R. S. Goldman, J. Appl. Phys. **114**, 043704 (2013).
[29] H. Zhao, M. Pokharel, S. Chen, B. Liao, K. Lukas, C. Opeil, G. Chen, and Z. Ren, Nanotechnology **23**, 505402 (2012).
[30] X. Zhou, G. Wang, L. Zhang, H. Chi, X. Su, J. Sakamoto, and C. Uher, J. Mater. Chem. **22**, 2958–2964 (2012).
[31] X. Zhao, H. Wang, S. Wang, D. Elhadj, J. Wang, and G. Fu, RSC Adv. **4**, 57148–57152 (2014).
[32] J. Zheng, J. Peng, Z. Zheng, M. Zhou, E. Thompson, J. Yang, and W. Xiao, Front. Chem. **3**, 53 (2015).
[33] N. Van Nong, N. Pryds, S. Linderoth, and M. Ohtaki, Adv. Mater. **23**, 2484–2490 (2011).
[34] Y. Wang, Y. Sui, J. Cheng, X. Wang, and W. Su, J. Alloys Compd. **477**, 817–821 (2009).
[35] M. Ito and J. Sumiyoshi, J. Jpn. Soc. Powder Powder Metall. **55**, 90–95 (2007).
[36] M. Ibáñez, R. J. Korkosz, Z. Luo, P. Riba, D. Cadavid, S. Ortega, A. Cabot, and M. G. Kanatzidis, J. Am. Chem. Soc. **137**, 4046–4049 (2015).
[37] L.-I. Hung, C.-K. Tsung, W. Huang, and P. Yang, Adv. Mater. **22**, 1910–1914 (2010).
[38] K. Kravchyk, L. Protesescu, M. I. Bodnarchuk, F. Krumeich, M. Yarema, M. Walter, C. Guntlin, and M. V. Kovalenko, J. Am. Chem. Soc. **135**, 4199–4202 (2013).